Analysis of Kinetic Energy Recovery System Based on Four-Phase Interleaved Buck Converter for Vehicle Verification Processes

Iván Reyes-Portillo, Abraham Claudio-Sánchez, Saul Méndez-Elizondo, Dora Castro-Lopez, and Luis Carreto-Hernández

***Abstract*—The automotive industry consumes large amounts of fossil fuels during vehicle acceleration and braking tests as part of quality verification. The kinetic energy generated in the test rollers is typically wasted during vehicle braking. One approach to reducing vehicle production costs and improving the efficiency of fossil fuel consumption is to recover a fraction of this energy using a system that does not interfere with vehicle verification standards. The recovered energy can be stored or used for other essential functions, such as powering lighting systems. In industrial processes, electrical energy is the most common form of energy recovery due to its advantages in storage, distribution, and transformation for various applications. This paper presents the analysis of a kinetic energy recovery system (KERS) based on a four-phase interleaved Buck converter for vehicle testing processes. A stage by stage analysis of the energy recovery system is provided, along with the selection of system parameters. Furthermore, the advantages of the proposed topology and the experimental results are discussed.**

Link to graphical and video abstracts, and to code: https://latamt.ieeer9.org/index.php/transactions/article/view/9490

***Index Terms*—Energy efficiency; Interleaved Buck converter; Flywheel; Kinetic energy; DC/DC, KERS.**

I. Introduction

GLOBAL warming, climate change, and ozone layer depletion are compelling governments to seek viable solutions to reduce fossil fuel consumption [1]. Automobile transportation is one of the primary sources of pollution due to the vast number of vehicles operating daily on roads worldwide [2]. While renewable energy sources have made significant advancements in recent decades, they remain insufficient to fully replace fossil fuels in industrial production processes [3]–[5]. The automotive industry requires substantial energy resources; however, these are often consumed inefficiently in manufacturing processes. Only $35\,\%$ of the energy utilized in these processes is effectively harnessed, while the remainder is lost due to factors such as friction, heat dissipation, steam, and leaks. This wasted energy can potentially be recovered and repurposed for secondary applications, such as lighting. Vehicle acceleration and braking tests require high kinetic energy, often leading to inefficient fossil fuel consumption. [7]. Additionally, various governmental institutions conduct vehicle verification tests to ensure that citizens maintain their vehicles in optimal condition [6], [8], [9]. Recovering kinetic energy from these processes not only mitigates environmental impact but also reduces production costs, which is a critical factor in maintaining a competitive industrial sector [10]. However, recovering residual energy presents significant challenges due to the complexity of certain processes. Kinetic energy recovery requires a system or mechanism that converts it into electrical energy [7]. Various kinetic energy recovery systems (KERS) have been presented in the literature. In [11]–[13], KERS based on flywheels, implemented directly in the vehicle's traction system, have been introduced, enhancing energy recovery efficiency. These KERS are primarily used in electric vehicles, which improves energy utilization; however, they also increase the vehicle's overall volume. A flywheel is a mechanical energy storage system whose main advantage over other systems is its ability to absorb and release energy within short time intervals [13]. This technology is particularly suitable for applications where energy is generated intermittently, requiring short energy transfer periods. In recent decades, the incorporation of composite materials in flywheel manufacturing has significantly increased their energy storage capacity [14], [15]. A major challenge in these systems is the integration between the power generation and storage stages. This integration requires a DC/DC converter that meets high power density requirements and is capable of handling high current levels. One solution proposed in the literature is the use of interleaved converters, which enable high current handling and improve power density in electronic systems by increasing the ripple frequency of reactive components. This paper presents the analysis of a kinetic energy recovery system (KERS) based on a four-phase interleaved buck converter. To ensure that standard vehicle verification processes remain unaffected, the recovered energy should primarily come from the flywheel rather than the rollers used during vehicle testing. Fig.1 shows the general scheme of the proposed KERS. The rollers, where vehicle verification tests are conducted, impose the speed conditions on the KERS, which is mechanically coupled to a flywheel via a unidirectional transmission. This

The associate editor coordinating the review of this manuscript and approving it for publication was Gabriel Pinto (*Corresponding author: Iván Alfonso Reyes-Portillo*).

Iván Alfonso Reyes-Portillo, and D. Castro are with the Universidad Politécnica de San Luis Potosí, San Luis Potosí, México (e-mail: ivan.reyes@upslp.edu.mx,and dora.castro@upslp.edu.mx).

A. Claudio-Sánchez is with the Centro Nacional de Investigación y Desarrollo Tecnológico, Cuernavaca, Morelos, México (e-mail: abraham.cs@cenidet.tecnm.mx).

S. Méndez-Elizondo is with the Universidad Autónoma de San Luis Potosí, San Luis Potosí, México (e-mail: saul.mendez@uaslp.mx).

L. Carreto-Hernández is with the Universidad Tecnológica de Gutiérrez Zamora, Veracruz, México (e-mail: luis.carreto@utgz.edu.mx).

one-way transmission also provides a beneficial transformation ratio to increase the flywheel speed. The rest of the paper is organized as follows: Section II presents the analysis of KERS operation, system modeling, and the speed transformation ratio. Section III details the design of each KERS stage, including the sizing of the recoverable energy capacity. Section IV introduces a minimum functional prototype, developed based on the design specifications obtained through simulation analysis. Finally, Section V provides concluding remarks.

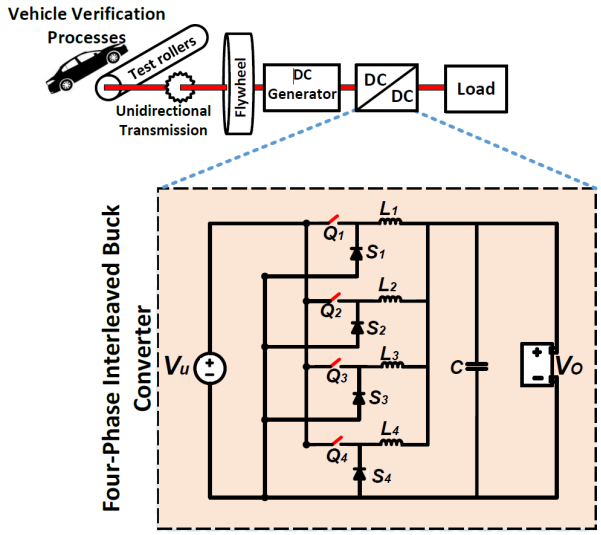

Fig. 1. Proposed KERS based on a Four-phase interleaved Buck converter for vehicle verification processes.

II. KERS Operation

The proposed KERS has two operating states, the "Acceleration state", consists of the acceleration of the vehicle on the test roller; during this state, the kinetic energy is stored in the flywheel. However, there is no energy transfer to the load, so as not to greatly modify the vehicle acceleration tests. The "Braking state" consists of braking the vehicle on the test roller; during this state, the unidirectional transmission disconnects the rollers from the flywheel. The kinetic energy stored in the flywheel is transformed by a DC generator and regulated by a DC/DC converter to the battery bank. Fig. 2 shows the KERS operating states during the vehicle verification process. During the "state of Acceleration", the angular speed of the flywheel will increase until the point where the vehicle starts to brake, at which time the flywheel will have reached its maximum angular velocity (ω_{max}). The ω_{max} is related to the maximum energy (E_{max}) stored in the flywheel. The voltage in the battery bank will be constant during this time and the current will decrease as the flywheel speed decreases. The type of roller used is a braking roller, with a diameter of 75 cm and a length of 210 cm. However, to emulate the speed conditions imposed by the rollers during the tests, a direct current motor coupled to the KERS was used.

A. Speed Profile in the Vehicle Verification Process

The amount of energy recovered should come mostly from the steering wheel and not directly from the rollers during

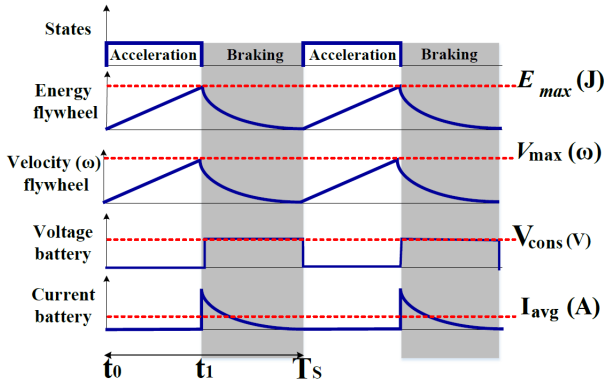

Fig. 2. Acceleration and braking operation modes of the proposed KERS.

vehicle testing. The flywheel must be sized to store the energy produced during acceleration tests, seeking the least impact to the standards in the tests. The vehicles are subjected to different speed conditions during the tests. Table I shows the test profile analyzed in a vehicle verification center, considering the speed reached by the vehicle and the time each test lasts. The diameter of the test rollers imposes a ratio of $7.2\,\mathrm{rpm}/(\mathrm{km\,h})$.

TABLE I
VEHICLE VERIFICATION TEST PROFILE UNDER ROLLER-IMPOSED SPEED CONDITIONS

Test	Speed (km/h)	Speed (rpm)	Test cycles	Test time (s)
1	60	435	720	7
2	80	576	720	7
3	100	720	720	7
4	120	864	720	7

Each test is performed an average of 720 times per day. The highest energy loss occurs when the vehicle reaches a speed of $120\,\mathrm{km/h}$ on the test rollers.

B. Modeling of the Proposed KERS

The proposed KERS is modeled to dimension the maximum energy that can be extracted from the system and to design the parts that integrate it considering the systems reported in [16]. Fig. 3 shows the block diagram of the KERS subsystems.

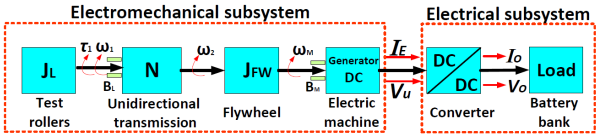

Fig. 3. Diagram of blocks that integrate the proposed KERS.

The modeling of the electromechanical subsystem is based on the relationship between the angular velocity of the rollers (V_u) and the output voltage (V_u). The angular velocity is imposed on a vehicular verification system, which eliminates the need to model torque-based inertial dynamics. The conversion from speed to rpm is done by a factor of 7.2. The transmission amplifies the speed of the rollers to match the

generator operation. The relationship between the roller speed and the speed at the flywheel input is expressed as:

$$w_2 = N \cdot w_1 \tag{1}$$

The flywheel model follows the equation of rotational dynamics based on Newton's second law for rotation:

$$J_{FW}\frac{d\omega_n}{dt} = \tau_2 - \tau_n - B_M\omega_n \tag{2}$$

where J_{FW} is the flywheel moment of inertia, B_M is the friction constant, τ_2 and τ_n are the input and output torques respectively. In Equation (3) the output torque is considered to be proportional to the output speed by a constant k_{out}:

$$\tau_n = k_{out}\omega_n \tag{3}$$

Similarly, input torque is assumed to be related to input speed through an ideal mechanical transmission.

$$\tau_1 = k_{in}\omega_1 \tag{4}$$

Substituting the torque equations into the flywheel dynamics Equation (2) and applying the Laplace Transform, the transfer function relating the input velocity to the output velocity is obtained.

$$G_{flywheel}(s) = \frac{\omega_n(s)}{\omega_1(s)} = \frac{k_{in}}{J_{FW}s + k_{out} + B_M} = \frac{K}{\tau s + 1} \tag{5}$$

where:

$$\tau = \frac{J_{FW}}{k_{out} + B_M}, \quad K = \frac{k_{in}}{k_{out} + B_M} \tag{6}$$

This equation represents a first order system with a time constant τ and a gain K, which describe the flywheel dynamics. Fig. 4 shows the DC generator used in the KERS design, as well as its electrical equivalent, on which its modeling is based. In addition, the inductance and armature resistance of the DC generator are presented.

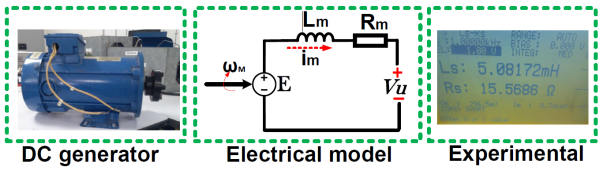

Fig. 4. DC generator used in the system and its equivalent electrical circuit.

The equivalent electrical circuit of the DC generator was analyzed with Kirchhoff's voltage law and the Equation (7) was obtained.

$$R_m i_m + L_m\frac{di_m}{dt} = E - V_u \tag{7}$$

The electromotive force is given by:

$$E \approx k_m\omega_M \tag{8}$$

Where k_g is the torque constant characteristic of DC motors and generators. The relationship between input speed and output voltage is obtained by applying the Laplace Transform to (7) and (8).

$$G_{gen}(s) = \frac{V_u(s)}{w_M(s)} = k_m \tag{9}$$

From Equations (1), (5) and (9), we obtain the transfer function relating the input speed w_1, expressed in km/h, to the generator output voltage V_u.

$$G_{em}(s) = \frac{V_u(s)}{w_1(s)} = G_{gen}(s) * G_{flyweel}(s) * N * 7.2 \tag{10}$$

III. Proposed KERS Design

This section presents the KERS design taking into account the speed characteristics imposed by the vehicles during the vehicle verification tests described in Table I. The design discusses the characteristics of the DC generator, the selection of the flywheel and the operation of the DC/DC converter. It also considers some weight and volume limitations on the flywheel so as not to affect the flywheel in the vehicle verification process.

A. DC Generator

The DC generator is a fundamental component for converting mechanical energy into electrical energy. A permanent magnet machine rated at 1800 rpm and 96 V was selected, with a nominal power of 1 kW. The unidirectional transmission has a transformation ratio of $N = 2.6$ to increase the speed between the test roller and the flywheel. The angular speed ω_m is provided by the flywheel. Based on the speed tests presented in Table I, the DC generator can be operated at rated speed conditions. Fig. 5 shows the velocity profiles at each stage of the subsystem from parameters obtained experimentally based on the transfer function (10).

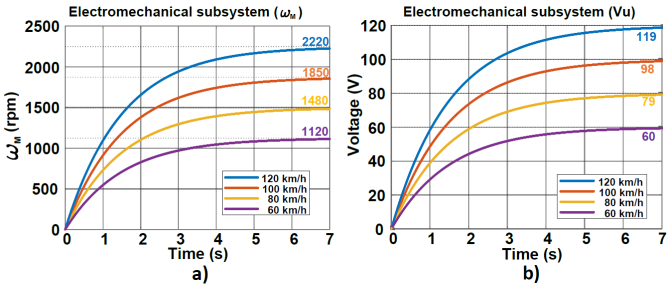

Fig. 5. Speed profiles at each stage of the system: a) relationship between roller speed and generator input speed and b) relationship between roller speed and generator output voltage.

B. Flywheel Selection

The flywheel is very important in the KERS operation, because the energy it stores during the "Acceleration state" is the one that will be transferred to the battery bank. The dimensioning of the flywheel is associated to the DC generator. The process of energy transfer to the battery depends on the speed conditions of the flywheel and therefore also of the generator due to its proximity. The higher the speed, the higher the generator output voltage and therefore the more energy transferred to the battery bank. Therefore, the flywheel design approximated the nominal operating speed of the DC

TABLE II
FLYWHEEL DESIGN VARIATIONS CONSIDERING MATERIAL, GEOMETRY AND ENERGY STORAGE

	r_1 (m)	r_2 (m)	m_{Steel} (kg)	m_{Alum} (kg)	J_{Steel} (kg m^2)	J_{Alum} (kg m^2)	E_{Steel} (J)	E_{Alum} (J)
Case 1	0.10	0.08	4.44	1.53	0.0364	0.0125	646.66	222.42
Case 2	0.15	0.13	6.91	2.38	0.1360	0.0468	2416.66	831.21
Case 3	0.20	0.15	21.58	7.42	0.6743	0.2319	11979.78	4120.43
Case 4	0.30	0.25	33.91	11.66	2.5856	0.8893	45933.89	15798.92
Case 5	0.30	0.20	62.65	21.20	4.007	1.3783	71190.50	24485.02

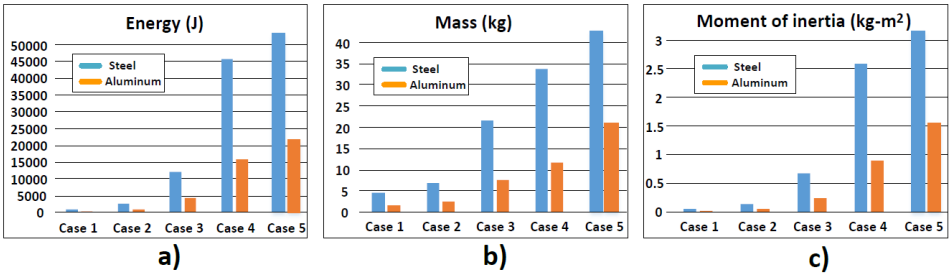

Fig. 6. Analysis of flywheel design cases, a) Energy, b) Mass, c) Moment of inertia.

generator. The stored kinetic energy is proportional to the flywheel speed and its moment of inertia. The angular velocity is higher as the stored energy of the flywheel increases, which is an important reason for operating flywheels at high rotational speeds. The energy of the flywheel is a function of the angular velocity and its moment of inertia, as defined by Equations (11) and (12).

$$E_{FW} = \frac{1}{2} J_{FW} (\omega_{2max}^2 - \omega_{2_{min}}^2) \tag{11}$$

where E_{FW} is the kinetic energy stored in the flywheel, J_{FW} is the moment of inertia (kg m^2), ω_{2max} is the maximum angular velocity (rad/s), and ω_{2min} is the minimum operating speed of the flywheel at which energy can be extracted. To reduce the mass of a flywheel, a suitable design for energy management is important. Based in Equations (11) and (12) the flywheel was designed.

$$J_{FW} = \frac{1}{2} m (r_1^2 + r_2^2) \tag{12}$$

$$m = v_m d_m \tag{13}$$

where m is the mass of the material, r_1 is larger flywheel radius, r_2 is smaller radius, v_m is the volume of the flywheel and d_m is the density of the material. The moment of inertia of a flywheel can be defined as a function of the flywheel size related to the mass and diameter specifications of the flywheel. Fig. 7 shows the flywheel designs analyzed for implementation in KERS considering the mass moments of inertia.

In Fig. 7 b), the moment of inertia is greater than in a), considering that a) and b) have the same mass and diameter but different radio, assuming the thickness of b) is greater. The inertia of flywheel b) is greater because the forces opposing the moment of inertia are smaller, which differs from the case where the flywheel has an equal mass distribution, as in design a). The flywheel was designed considering the characteristics of b), and as a result, the design presented in Fig.7 c) was obtained. Table II shows the design cases

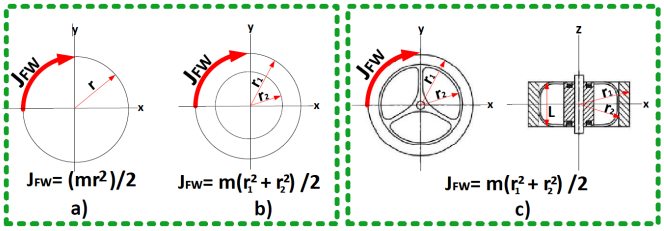

Fig. 7. Structural design of the flywheel, a) flywheel with uniform mass, b) flywheel with the highest mass on the external perimeter, and c) design of the selected flywheel.

studied for the flywheel by varying the radius and material parameters. The materials selected for this analysis were steel and aluminum due to their cost-effectiveness and high energy storage capacity resulting from their moments of inertia. Fig. 6 shows the analysis of each case studied in Table II, where the energy storage capacity, mass and moment of inertia of the design case were considered. Cases one and two are the ones that can store the least energy, so they are not suitable for KERS due to the speeds achieved in each acceleration test. Cases four and five would be the most suitable due to their storage capacity and moment of inertia. However, these designs require high mass values, which directly affects the acceleration tests by increasing the energy consumption of the vehicle and impacting the test standards. Due to these considerations, a flywheel with the characteristics of case three and made of steel was designed. A key point in the selection of the flywheel material is the power density, due to the limited space in the acceleration test rollers, so case three was chosen.An additional advantage of steel is its higher wear and fatigue resistance compared to aluminum, which prolongs the service life of the flywheel in high-demand applications. In terms of cost, although aluminum is lighter and can facilitate manufacturing in certain cases, steel is usually more economical and is widely available in various alloys

optimized to withstand high mechanical stresses.

C. Four-phase Interleaved Buck Converter

Due to the speed conditions imposed by the test rollers at the generator input, the most optimal way to store energy is to reduce the voltage levels and increase the current in the battery bank to take advantage of the voltage ranges during flywheel speed reduction. The KERS requires a Buck converter to maintain high current levels and proper voltage regulation. However, Buck converters have the disadvantage of presenting a discontinuous current demand to the DC generator, which reduces the useful life of the electric machine. One solution to this problem is the implementation of an LC filter; however, this affects the power density of the converter [17]. One solution to this problem is to employ a Buck interleaved converter that operates with overlapping duty ratios to eliminate the discontinuous current demand on the DC generator. An advantage of interleaved converters is the distribution of the output current among the inductors in each phase. This reduces the size of the inductor and increases the power density of the converter. Additionally, it increases the frequency of current and voltage ripple at the converter output, which reduces the size of the output capacitor [18], [21]. Another advantage of Buck Interleaved converters is that they maintain their minimum phase characteristics, meaning they do not have zeros on the right-hand side of the s plane, which facilitates voltage regulation [20]. Fig. 1 shows the Four-Phase Interleaved Buck (FPIB) converter, designed to transfer the energy recovered from the DC generator to the battery bank. The FPIB converter, designed to manage the energy recovered by KERS to the battery bank, has eight operating states during one switching period (T_s) as shown in Fig. 8.

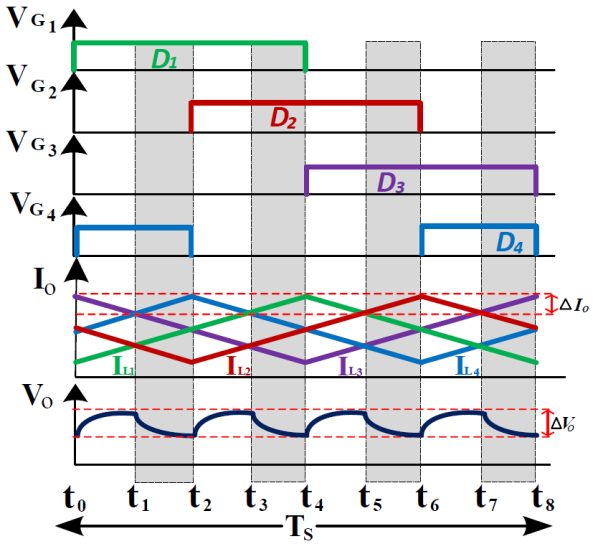

Fig. 8. Voltage and current waveforms during one switching period (T_s) of the four-phase interleaved Buck converter, showing gate signals V_{G1}–V_{G4}, inductor currents I_{L1}–I_{L4}, and output voltage V_o.

Due to the 90° phase shift between the control signals, the operating dynamics of the converter is improved by reducing the output current ripple and voltage ripple. The frequency of voltage and current ripple at the output is also increased by the ripple cancellation effect. In the quadruple interleaved structure, it is important to operate with duty ratios higher than 25 % to eliminate the discontinuous current at the input of the converter. The ripple cancellation effects and the operation of the control signals are shown in Fig. 8 with the waveforms at one switching period (T_S). To obtain an effective voltage transformation ratio for CCM, the volt-second balance of the voltage signal in one of the inductors is applied, considering that the duty ratio (D) is the same in each phase. The voltage transformation ratio is given by:

$$M = \frac{Vo}{V_U} = D \tag{14}$$

The following expressions establish the value of the inductance that the converter needs in each phase to operate in its steady state. It is important to consider the percentage of the current ripples (Δ_{I_L}) according to the load. Equations (15-18) size the value of inductors in the FPIB converter .

$$L_1 = \frac{V_o(1-D_1)}{\Delta I_{L_1} f_s} \tag{15}$$

$$L_2 = \frac{V_o(1-D_2)}{\Delta I_{L_2} f_s} \tag{16}$$

$$L_3 = \frac{V_o(1-D_3)}{\Delta I_{L_3} f_s} \tag{17}$$

$$L_4 = \frac{V_o(1-D_4)}{\Delta I_{L_4} f_s} \tag{18}$$

To determine the value of the capacitor, it is necessary to consider the converter output frequency ($f_{S_{out}}$) given by the Equation (19).

$$f_{S_{out}} = 4fs \tag{19}$$

The output frequency is four times higher than the switching frequency (f_s) as a result of the ripple cancellation effect. Consequently, the output capacitor reduces its capacitance value considerably. The value of the capacitor is determined by Equation (20).

$$C = \frac{V_o(1-D_1)D_1}{8\Delta V_C L_1 f_{S_{out}}^2} \tag{20}$$

Table III presents the design parameters of the FPIB converter for CCM operation. Fig. 9 shows the current and voltage waveforms of the FPIB converter obtained in the Powesim simulator, considering the parameters presented in Table III and a duty ratio of 50 %, since this is the point of greatest energy stress to which the converter will be subjected.Fig. 9 shows the current and voltage waveforms of the FPIB converter obtained in the Powesim simulator, considering the parameters presented in Table III and a duty ratio of 50 %, since this is the point of greatest energy stress to which the converter will be subjected. The input current was compared with a conventional converter considering the same operating conditions.

It is observed that the FPIB converter current presents a continuous current demand to the generator, while the Buck conventional converter presents a discontinuous input current.

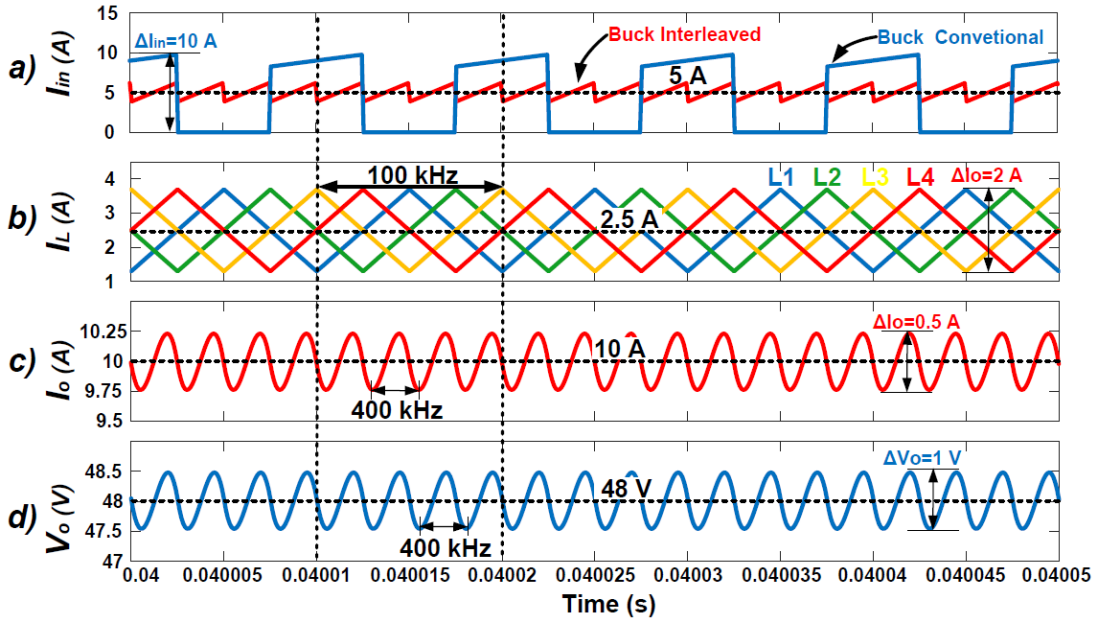

Fig. 9. Current and voltage waveforms obtained in the simulation, considering the highest power voltage point, a) input current, b) inductor current, c) output current and d) output voltage.

TABLE III
DESIGN PARAMETERS OF THE FOUR-PHASE INTERLEAVED BUCK CONVERTER

Symbol	Parameter	Value
V_G	Input voltage	55 V – 100 V
V_o	Output voltage	48 V
P_o	Output power	480 W
I_o	Output current	10 A
f_s	Switching frequency	100 kHz
L_{1-4}	Inductors	150 µH
C_o	Output capacitor	1 µF
D	Duty cycle	50% – 87%
Q_{1-4}	MOSFETs	C20N60CFD
S_{1-4}	Diodes	TO-220-L

The discontinuous current of the Buck conventional converter has a maximum value of 10 A.

The discontinuous current decreases the lifetime of the generator, so it is not suitable for this type of application. The currents in the inductors have a frequency of 100 kHz for each phase and a current ripple of 2 A. The output current is 10 A, with a frequency of 400 kHz and a current ripple 0.5 A due to the ripple cancellation effect. The converter output voltage is 48 V with a frequency of 400 kHz, this effect benefits in decreasing the capacitor size, as shown in Equation (20).

IV. RESULTS

To validate the results, a working prototype was designed. Fig. 10 shows the KERS platform, which integrates the electromechanical components, including a test roller emulator, a unidirectional transmission, a flywheel, and a DC generator. Instead of physical test rollers, a DC motor was used to replicate the torque and speed conditions typically found in vehicle verification processes. The test roller emulator is programmed to provide the different speed profiles presented in Table I, ensuring controlled experimental conditions equivalent to those of a standard testing environment.

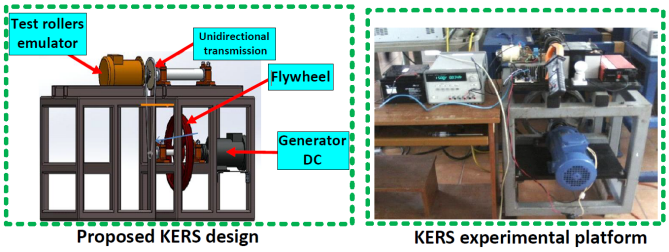

Fig. 10. Experimental platform of the electromechanical structure of KERS.

Fig. 12 shows the prototype of the FPIB converter integrated to the output terminals of the DC generator. This work proposes the current equalization in each phase of the converter by means of a hysteresis controller that integrates voltage regulation, current balancing and a 90° phase shift in the control signals. These functions are implemented through the commercial controller ISL6558 [22]. The design prioritizes simplicity, low cost and efficiency. Voltage regulation only requires measurement of the output voltage, while current balancing is achieved by measuring the voltage at each switch.

This scheme was presented in [19] for the analysis of current imbalance effects. The Fig. 12 presents the thermal spectra of the converter Q_{1-4} switches operating at the maximum stress point during the energy recovery process. During current balancing, the temperature of the transistors varies in the range of 49.1 °C to 59.5 °C, which directly influences the efficiency of the converter. However, the advantages in terms of power density and high current handling compensate for the overall system efficiency. Fig. 11 shows the results obtained in the proposed FPIB for KERS. Fig. 11 a) show the duty ratio in

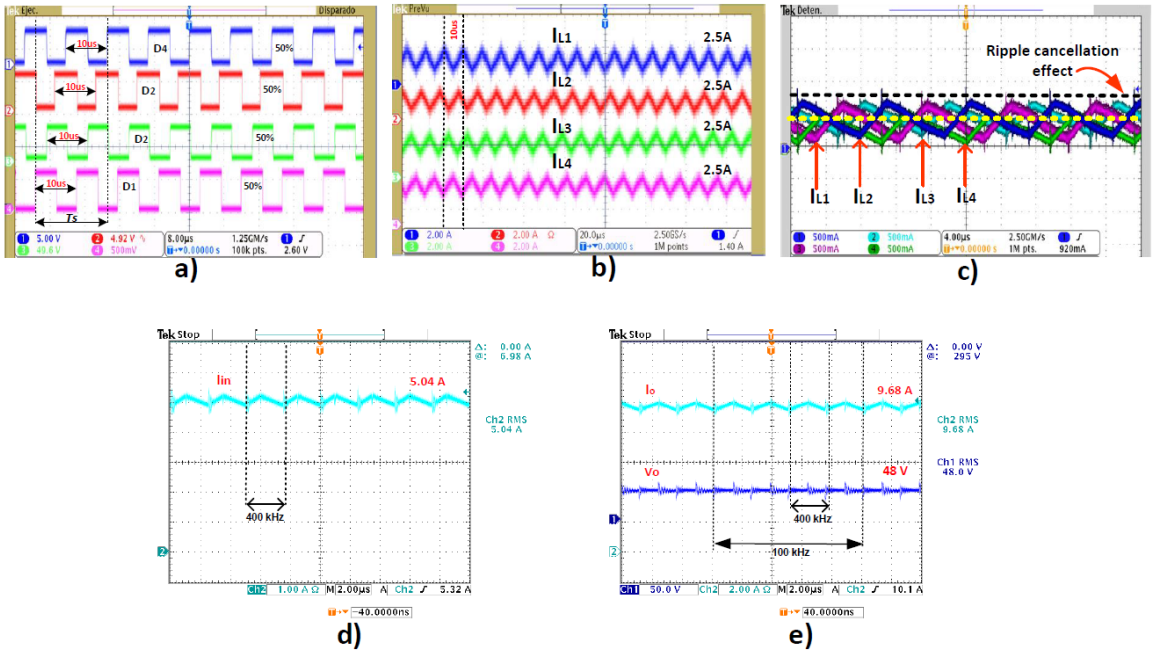

Fig. 11. Experimental waveforms of the FPIB converter, a) Duty ratio control signals operating at 50 %, b) currents in the inductors of each phase, c) ripple cancellation effect obtained with the phase shift of the inductor currents, d) current at the input of the converter and d) voltage and current at the output of the converter.

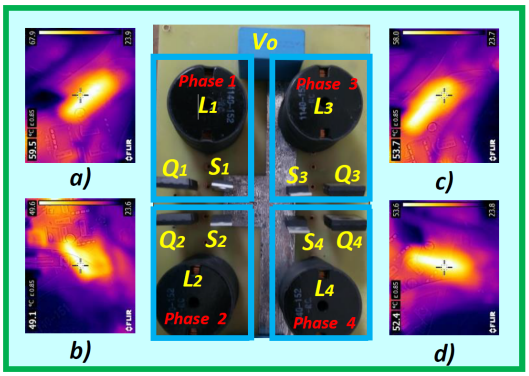

Fig. 12. Prototype of the FPIB converter y los espectros de temperatura en los interruptores Q_{1-4}: a) Q_1, b) Q_2, c) Q_3 and a) Q_4.

each phase, with an offset between each phase of 90° and a frequency of 100 kHz.

Fig. 11 b) depects the inductor current for each phase of the FPIB converter. The current per phase is 2.5 A with a ripple of 100 kHz in each phase. Fig. 11 c) shows the effect of ripple cancellation on the converter output current. This effect allows to increase the current/voltage ripple value at the output of the converter. This effect allows the converter to be designed with high levels of current ripple in the inductors of each phase, to increase the power density of the converter. Fig. 11 d) shows the continuous current at the converter input due to the ripple cancellation effect of the control signals.

The current remains continuous only when the converter operates with duty cycles greater than 25 %. The input current is 5.04 A and at a frequency of 400 kHz. Fig. 11 d) shows the converter output current and voltage at the point of highest energy stress that can operate in KERS. The output voltage is 48 V and the output current is 9.68 A. The ripples in the output current and voltage have a frequency of 400 kHz due to the ripple cancellation effect. Fig. 13 shows the efficiency of the FPIB converter in different power output scenarios. The proposed converter at the nominal power of 480 W presented an efficiency of 92 %. A factor of great relevance to efficiency is the current equalization in each phase as shown in a previous study presented in [19]. This paper presents results of the converter in the current balance in each phase. Fig. 14 shows the FPIB converter ratings for each component operating at 480 W nominal power.

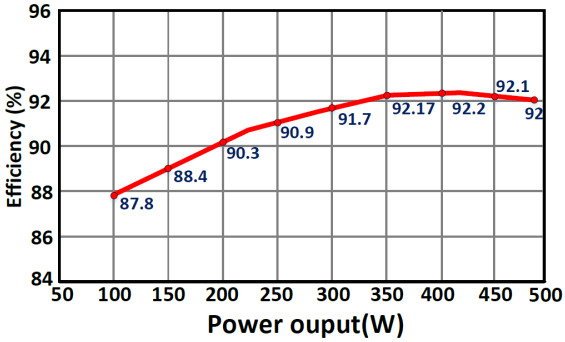

Fig. 13. Efficiency of the FPIB converter with different output power values.

A. Discussions

For the analysis of the recovered energy, the operating conditions of the DC/DC converter were considered where the maximum voltage obtained by the generator is 100 V and

TABLE IV
COMPARISON OF KINETIC ENERGY RECOVERY SYSTEMS (KERS)

KERS	Flywheel/Material	Converter Type	Energy (J)	Power (W)	Application	Max Speed (km/h)	Efficiency
Proposed	Yes / Steel	Interleaved Buck	2959	450	Verification	120	91%
Ref [23]	Yes / X	Interleaved Buck-Boost	18 700	2400	Vehicle	50	92 %
Ref [24]	Yes / X	Boost	308 000	50 000	Vehicle	120	80 %
Ref [25]	Yes / Steel	Three-phase DC–AC	X	50 000	Vehicle	51.5	99 %
Ref [26]	No / X	Bidirectional Inverter	X	23 000	Industrial Plant	X	92 %
Ref [27]	Yes / X	Bidirectional Inverter	3 125 000	720	Vehicle	X	93 %

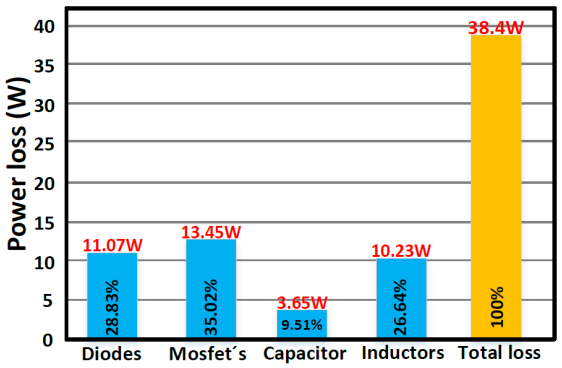

Fig. 14. Power losses in the converter components during nominal power operation.

the minimum voltage is 55 V, in order to maintain the duty ratio in operating ranges from 50 % to 85 %. In different tests presented in Table I, it was possible to extract approximately 2792 J in test one, 2680 J in test two, 2958 J in test three and 1876 J in test four. However, each test is performed 720 times per day. Fig. 15 shows the energy recoverable in each test, a) during one day in terms of jouls, b) in terms of wh and c) the total energy obtained is approximately 9,406 watts per hour in five working days. The results obtained indicate that gasoline consumption during each test is approximately 0.048 liters in a period of 37 seconds, at an average speed of 80 km/h. Extrapolating this consumption to 720 daily tests, a total expenditure of 34.5 liters of fuel per day is estimated. In addition, it has been shown that, to recover an amount of energy of 9406 W h, fuel consumption increases by 22 %, which significantly impacts the cost of the energy recovered. Table IV presents a comparison of KERS as a function of flywheel material, type of converter used, stored energy, power output, application, maximum speed and efficiency. The proposed system employs a steel flywheel and an Interleaved Buck converter, achieving an efficiency of 91 % in the power stage with a storage capacity of 2959 J and an output power of 450 W. Compared to literature references, it is observed that other KERS use different converter configurations, such as Boost, Interleaved Buck-Boost and bidirectional converters, in addition to various applications ranging from vehicles to industrial plants. While most of these applications allow for higher power recovery, they also have higher losses. The proposal offers competitive efficiency relative to other structures and greater complexity in the energy recovery process.

V. CONCLUSION

This paper has analyzed a kinetic energy recovery system (KERS) based on a four-stage interleaved Buck converter, which uses a flywheel as an energy storage medium. This system proves to be an effective solution for energy recovery in applications such as vehicle verification, where efficiency in energy conversion and storage is key to improving performance and reducing energy consumption. The implementation of a four-phase interleaved converter allows precise control of the recovered energy, optimizing both power and system stability, as well as improving power density. The use of the flywheel as a storage device provides advantages in terms of storage capacity and rapid response to fluctuations in vehicle load, making it an attractive option for processes that require high energy recovery rates. In addition, the interleaved converter architecture helps to minimize energy losses and improve overall system efficiency. This approach is promising not only for vehicle applications, but also in other industrial sectors where energy efficiency and energy recovery are essential. The integration of advanced technologies such as KERS based on flywheels and interleaved converters could play a crucial role in the transition to more sustainable and environmentally friendly transportation systems.

ACKNOWLEDGMENTS

The authors are grateful to the Secretaría de Ciencias, Humanidades, Tecnología e Innovación (SCHTI).

REFERENCES

[1] M. Aien and O. Mahdavi, "On the way of policymaking to reduce the reliance of fossil fuels: Case study of Iran," Sustainability, vol. 12, no. 24, p. 10606, 2020; doi:https://doi.org/10.3390/su122410606.
[2] M. A. Rahim et al., "Evolution of IoT-enabled connectivity and applications in the automotive industry: A review," Veh. Commun., vol. 27, p. 100285, 2021; doi:https://doi.org/10.1016/j.vehcom.2020.100285.
[3] B. Doğan and D. Erol, "The Future of Fossil and Alternative Fuels Used in Automotive Industry," 2019 3rd International Symposium on Multidisciplinary Studies and Innovative Technologies (ISMSIT), Ankara, Turkey, 2019, pp. 1-8, doi: 10.1109/ISMSIT.2019.8932925.

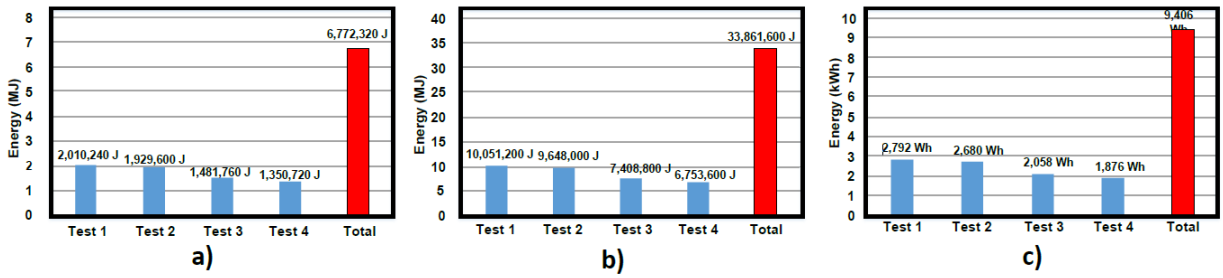

Fig. 15. Energy recovered in the different verification tests: a) Energy in one day (Joules), b) Energy in five days (Joules), c) Energy in five days (W h).

[4] I. A. Reyes-Portillo, J. Morales-Saldaña, C. Romero-Rivera and E. Palacios-Hernández, "Design and Modeling of a High Current Ratio Converter for PV Applications," in IEEE Latin America Transactions, vol. 21, no. 10, pp. 1144-1155, Oct. 2023, doi: 10.1109/TLA.2023.10255452.

[5] I. A. Reyes-Portillo, J. A. Morales Saldaña, E. M. Netzahuatl-Huerta and R. Loera-Palomo, "Design and Analysis of Quadratic Buck Converter Based on the Reduced Redundant Power Processing," in IEEE Journal of Emerging and Selected Topics in Power Electronics, vol. 12, no. 1, pp. 803-814, Feb. 2024,doi: 10.1109/JESTPE.2023.3322707.

[6] Razdan, Rahul. Unsettled technology areas in autonomous vehicle test and validation. No. EPR2019001. SAE Technical Paper, 2019, doi: https://doi.org/10.4271/EPR2019001.

[7] I. Reyes, A. Claudio, E. Flores and M. Lopez, "Analysis of kinetic energy recovery system based on inertial flywheel," 2018 14th International Conference on Power Electronics (CIEP), Cholula, Puebla, Mexico, 2018, pp. 130-136, doi: 10.1109/CIEP.2018.8573357.

[8] B. A. Raji, Assessment of vehicle inspection services in Ijebu zone of Ogun State, Nigeria, Ethiopian Journal of Environmental Studies and Management, vol. 9, no. 2, pp. 179–196, 2016, doi: 10.4314/ejesm.v9i2.6.

[9] S. AlKheder, F. AlRukaibi, and A. Aiash, "Vehicle inspection policy and emission analysis in Kuwait," Environmental Geochemistry and Health, vol. 42, pp. 3415–3429, 2020, doi: 10.1007/s10653-020-00584-5.

[10] H. S. Mann and P. K. Singh, "Kinetic energy recovery from the chimney flue gases using ducted turbine system," Chinese Journal of Mechanical Engineering, vol. 30, pp. 472–482, 2017, doi: 10.1007/s10033-017-0090-8.

[11] W. Zhang and J. Yu, "Modeling of vehicle-mounted flywheel battery considering automobile suspension and pulse road excitation," Energies, vol. 16, no. 11, p. 4288, 2023, doi: 10.3390/en16114288.

[12] P. Ji, W.-W. Nie, and J.-L. Liu, "Research on magnetic coupling flywheel energy storage device for vehicles," Applied Sciences, vol. 13, no. 10, p. 6036, 2023, doi: 10.3390/app13106036.

[13] W. Zhang and Z. Wang, "Dual-Mode Coordinated Control of Magnetic Suspension Flywheel Battery Based on Vehicle Driving Conditions Characteristics," in IEEE Transactions on Transportation Electrification, vol. 10, no. 1, pp. 2124-2134, March 2024, doi: 10.1109/TTE.2023.3288730.

[14] F. A. Ilmiawan and S. A. Zaki, "Application of flywheel energy storage on generator-set," Journal of Advanced Research in Fluid Mechanics and Thermal Sciences, vol. 105, no. 2, pp. 78–87, 2023, doi:10.37934/arfmts.105.2.7887.

[15] D. Zhai, L. Yao, S. Liao, J. Xu, B. Mao and B. Xie, "Modeling and Control of Flywheel Energy Storage System," 2023 6th International Conference on Electronics Technology (ICET), Chengdu, China, 2023, pp. 1289-1293, doi: 10.1109/ICET58434.2023.10211639.

[16] Jianguo Wang, Jianhui Su, Jidong Lai, Jian Zhang and Shuya Wang, "Research on control method for flywheel battery energy storage system," 2016 IEEE 8th International Power Electronics and Motion Control Conference (IPEMC-ECCE Asia), Hefei, 2016, pp. 1006-1010, doi: 10.1109/IPEMC.2016.7512424.

[17] I. A. Reyes-Portillo, J. A. Morales-Saldaña, E. M. Netzahuatl-Huerta, E. R. Palacios-Hernández and S. R. Méndez-Elizondo, "Modeling of a Quadratic Buck Converter Based on the R2P2 Concept for PV Applications," 2020 IEEE International Autumn Meeting on Power, Electronics and Computing (ROPEC), Ixtapa, Mexico, 2020, pp. 1-6, doi: 10.1109/ROPEC50909.2020.9258753.

[18] J. Gordillo and C. Aguilar, "A Simple Sensorless Current Sharing Technique for Multiphase DC–DC Buck Converters," in IEEE Transactions on Power Electronics, vol. 32, no. 5, pp. 3480-3489, May 2017, doi: 10.1109/TPEL.2016.2592240.

[19] I. A. Reyes-Portillo *et al.*, "Study of the effects of current imbalance in a multiphase buck converter for electric vehicles," World Electric Vehicle Journal, vol. 13, no. 5, p. 88, 2022, doi:10.3390/wevj13050088.

[20] X. Ding, Z. Zhao, Z. Shan and X. Song, "A Real-Time Sinusoidal Voltage-Adjustment Power Supply System Based on Interleaved BUCK Converters With Enhanced Reference-Tracking Capability," 2021 IEEE Energy Conversion Congress and Exposition (ECCE), Vancouver, BC, Canada, 2021, pp. 4810-4814, doi: 10.1109/ECCE47101.2021.9595946.

[21] A. Chawla and M. Kumar, "Design and Control of Fault-Tolerant Interleaved Buck Converter for Battery Charging Applications," 2023 International Conference on Power, Instrumentation, Control and Computing (PICC), Thrissur, India, 2023, pp. 1-6, doi: 10.1109/PICC57976.2023.10142844.

[22] Renesas, "ISL658 multi-purpose precision multi-phase PWM controller with optional active voltage positioning," Datasheet, 2015. [Online]. Available: doi:https://www.renesas.com/us/en/document/dst/isl6558-datasheet.

[23] G. Vitale and E. Pipitone, "A Six Legs Buck-boost Interleaved Converter for KERS Application," Renew. Energy Power Qual. J, vol. 18, no. 5, pp. 461-468, 2020; doi: 1https://doi.org/10.24084/repqj18.382.

[24] N. Farrokhzad Ershad, R. Tafazzoli Mehrjardi and M. Ehsani, "High-Performance 4WD Electric Powertrain With Flywheel Kinetic Energy Recovery," in IEEE Transactions on Power Electronics, vol. 36, no. 1, pp. 772-784, Jan. 2021, doi:10.1109/TPEL.2020.3004866.

[25] A. De Bernardinis, R. Lallemand, and A. Kolli, "Highly efficient three-phase bi-directional SiC DC–AC inverter for electric vehicle flywheel emulator," Energies, vol. 16, no. 12, p. 4644, 2023, doi: 10.3390/en16124644.

[26] A. D. S. Lima, A. R. Guedes, E. M. Sa and F. L. M. Antunes, "Case Study: Variable-Voltage DC Bus With Energy Recovery System for Industrial Plants," in IEEE Access, vol. 9, pp. 101277-101288, 2021, doi: 10.1109/ACCESS.2021.3095754.

[27] N. Farrokhzad Ershad, R. Tafazzoli Mehrjardi and M. Ehsani, "Efficient Flywheel-Based All-Wheel-Drive Electric Powertrain," in IEEE Transactions on Industrial Electronics, vol. 68, no. 7, pp. 5661-5671, July 2021, doi: 10.1109/TIE.2020.2992942.

Iván Alfonso Reyes-Portillo (member IEEE) received the degree of Electromechanical Engineer from the Instituto Tecnológico Superior de San Andrés Tuxtla, San Andrés Tuxtla, Veracruz, México in 2016 and the degree of Master of Science in Electronic Engineering from the Centro Nacional de Investigacion Y Desarrollo Tecnológico, Cuernavaca, Morelos, México in 2019. Obtained a Ph.D. in Electrical Engineering from the Universidad Autónoma de San Luis Potosí, San Luis Potosí, México, in 2024. He is currently a professor at Universidad Politécnica de San Luis Potosí in the Academy of Engineering in Systems and Industrial Technologies. His main areas of interest are DC/DC converters, redundant power processing converters, energy storage and renewable energies.

Abraham Claudio Sanchéz (member IEEE) received the B.Sc. degree and M.Sc. degree in electrical engineering from the Technological Institute of Laguna, Torreón, Coahuila, México, in 1983 and 1987, respectively, the advance studies degree (DEA), and the Ph.D. degree in electrical engineering (power electronics) from the National Polytechnic Institute of Grenoble (INPG), Grenoble, France, in 1992 and 1995, respectively.,He was a Postdoctoral Researcher with the Center for Power Electronics Systems, Virginia Polytechnic Institute and State University, Blacksburg, in 2002. Since 1987, he has been with the National Center for Research and Technological Development (cenidet), Cuernavaca, Morelos, Mexico, as a full-time Professor in the Power Electronics Group. His field of major interest and experience is characterization and modeling of power-semiconductor devices, and he has affinity with other related topics like ac motor control and fault detection.

Saúl Rolando Méndez-Elizondo (member IEEE) received the degree of Biomedical Engineer and the degree of Master´s in Electrical Engineering from the Universidad Autónoma de San Luis Potosi, San Luis Potosí, Mexico, in 2017 and 2020, respectively. He is currently a PhD. student in Electrical Engineering at the Autonomous University of San Luis Potosí. His main areas of interest are DC/DC converters, study of stability in DC microgrids, energy storage and controller design for power electronic systems.

Dora Luz Castro-López received the B.S. degree in mechanical engineering from the Universidad Autónoma de Zacatecas (UAZ), Zacatecas, in 2011, and the master's and Ph.D. degrees in mechanical engineering from the Universidad Autónoma de San Luis Potosí (UASLP), San Luis Potosí, México, in 2014 and 2021, respectively. She is currently a professor at Universidad Politécnica de San Luis Potosí in the Academy of Engineering in Systems and Industrial Technologies. His research interests focus on heat transfer in biomedical systems and fluid mechanics applications. In addition, she is interested in the study of heat transfer and thermal design of power electronics systems.

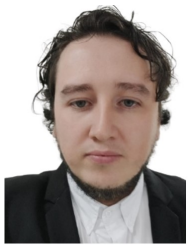

Luis Guillermo Carreto-Hernández received the degree in Electromechanical Engineering from the Instituto Tecnológico Superior de Misantla (ITSM) in 2016. In 2019 and 2023, he completed his Master's and PhD degrees in Mechanical Engineering Sciences at the Centro Nacional de Investigación y Desarrollo Tecnológico (CENIDET). He is currently a professor at the Universidad Tecnológica de Gutiérrez Zamora (UTGZ).